Hyperfine Interact (2018) 239:16
https://doi.org/10.1007/s10751-018-1492-4

The effect of Zn substitution on the structure and magnetic properties of magnesium nickel ferrite

Abbasher M. Gismelseed[1] · K. A. Mohammed[2] · F. N. Al-Mabsali[1] · M. S. Al-Maashani[1] · A. D. Al-Rawas[1] · A. A. Yousif[1] · H. M. Widatallah[1] · M. E. Elzain[1]

Abstract The series $Zn_xMg_{1-x}NiFeO_4$($0.0 \leq x \leq 1.0$) were prepared by the conventional solid state double sintering ceramic techniques and studied using X-ray diffraction (XRD), and Mössbauer spectroscopy techniques. The diffraction patterns of all samples show single phase cubic spinel structure. Mössbauer spectroscopy measurements at liquid nitrogen temperature show an ordered magnetic structure with well resolved tetrahedral and octahedral sites. Data analysis were performed in order to investigate the magnetic properties of the materials and their cation distribution behavior between the tetrahedral and octahedral sites. These will be discussed based on the substitution of both diamagnetic divalent.

Keywords Mössbauer · Spin canting · Effective magnetic moment · Cation distribution

1 Introduction

Due to their, low eddy current losses, moderate permittivity, high resistivity and, high permeability, the insulating magnetic oxide, spinel ferrites are becoming the subject of interest in theoretical as well as technological applications. Most of the physical properties of the spinel ferrites have been strongly influenced by the methods of preparation and heat treatment. The dominant magnetic super exchange inter-sublattice interaction in the spinel

This article is part of the Topical Collection on *Proceedings of the International Conference on the Applications of the Mössbauer Effect (ICAME 2017), Saint-Petersburg, Russia, 3-8 September 2017*
Edited by Valentin Semenov

✉ Abbasher M. Gismelseed
abbasher@squ.edu.om

1 Department of Physics, College of Science, Sultan Qaboos University, P.O. Box 36, Code 123, Al-khoud, Oman

2 Department of Mathematical and Physical Sciences, College of Arts & Sciences, University of Nizwa, P.O. Box 33, Code 616, Nizwa, Oman

Published online: 08 February 2018

ferrite is the (A)-O-[B] interaction, which is mostly twenty fold stronger than the intra-sublattices [B]-O-[B] and (A)-O-(A) interactions [1]. Nickel ferrite is a magnetic material of much important technological applications. To understand its exchange interaction, crystallographic lattice structure and magnetic properties it is always preferable to mix it by different magnetic or diamagnetic ions [2].

This work reports on the compositional dependence of the structural and magnetic properties of Zn^{+2} substituted Mg-Nickel ferrite having the general chemical formula $Zn_xMg_{1-x}NiFeO_4$ (x= 0.0 to 1.0 step 0.2), using the XRD, VSM and Mössbauer spectroscopy.

2 Experimental

The series of the $Zn_xMg_{1-x}NiFeO_4$ (x= 0.0 to 1.0 step 0.2) ferrites were prepared by the conventional double sintering ceramic technique as described earlier [3]. The purity, and homogeneity of each of the studied samples as well as their cells lattice constants are determined by X-ray powder diffraction patterns (XRD) using Phillips PW1820 diffractometer with CuKα radiation (λ =1.5404 Å). The Rietveld method using the FULLPROF software is applied to determine the structural analysis of the series [4]. The scan ranges were kept the same for all samples ($2\theta = 20^o$-80°) using a step size of 0.02^o with sample time of 2 s.

Magnetization as a function of the temperature in an applied magnetic field of 0.05 T and also as a function of magnetic field (1.3 T; max.) were measured using a vibrating sample magnetometer (VSM). Mössbauer spectra were obtained at 295 K and 78 K on a powdered sample using a constant acceleration spectrometer with 50 mCi ^{57}Co in Rh source. The low temperature measurements were performed using a liquid nitrogen flow cryostat. The spectrometer was calibrated with an α-Fe foil spectrum at 295 K. The measured data were analyzed using recoil program for a non-linear least-square fitting assuming Lorentzian lines for discrete sites [5].

3 Results and discussion

X-ray powder diffraction pattern of the series depicted in Fig. 1 revealed that all studied samples could be indexed in terms of a single phase cubic spinel with no additional phases. The structural analysis details are obtained by using the Rietveld methods program which confirm the homogeneity of the single phase (space group Fd-3m No. 227) of the samples. Relevant refinement data for one of the series are collected in Table 1, and plotted in Fig. 2. In Table 2 the experimental lattice parameters of the series are listed. The increase of the lattice parameter with increasing the Zn content is related to the replacement of Mg^{2+} ion of ionic radius 0.650 Å by Zn^{2+} which has larger ionic radius of 0.740Å.

The Magnetization hysteresis curves of the studied series measured at room temperature and applied field between -1300 and +1300 Oe are plotted in Fig. 3. The saturation magnetization of each concentration is calculated by extrapolating the data of magnetization M versus the reciprocal of the applied field 1/H. As shown in Fig. 3, the saturation magnetization increases smoothly from x = 0.0 to 0.6 reaching the maximum value of 10.6 emu/g for x = 0.6 composition and then decreases gradually while Zn contents increases. To understand such behavior the saturation magnetization are used to calculate the experimental magnetic

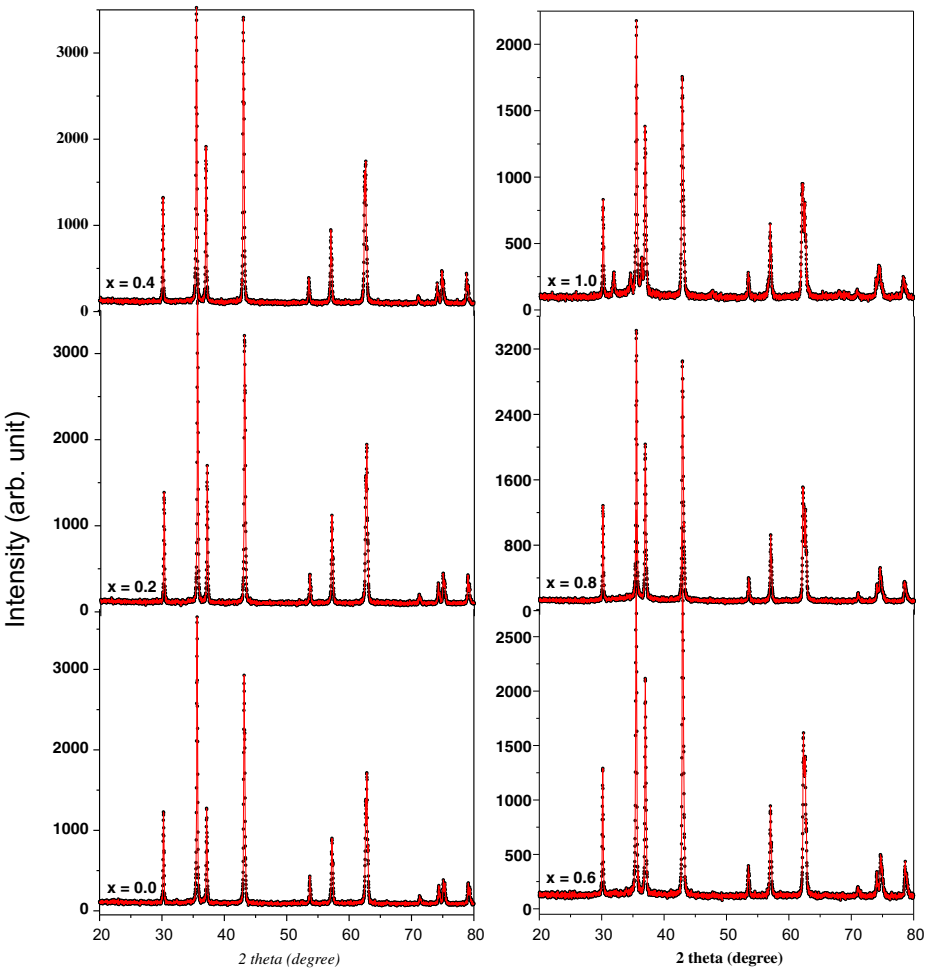

Fig. 1 The X-ray diffraction patterns of $Zn_xMg_{1-x}NiFeO_4 (0.0 \leq \times \leq= 1.0)$

moment in Bohr magneton per formula unit using the relation: $\mu_B = \frac{MWxM_s}{5585}$ where MW is the molecular weight of each composition and M_s is its saturation magnetization [6]. The results are plotted in Fig. 4.

In the cubic mixed Mg/Zn Ni-spinel ferrite, the diamagnetic Zn^{2+} ions reside preferentially in the A-site replacing the diamagnetic Mg^{2+} ion and the Fe^{3+} ($\mu_B = 5$) leading to the reduction of the magnetic moment of the A-sublattice. According to the Neel's two sublattices model, the net magnetization, which is the vector sum of the magnetic moments of the two sublattices, will increase within the region of $0 \leq x \leq 0.6$. However, as shown in Fig. 4, magnetization decreases at higher level of doping and no longer following the Neel's model. The reason for this behavior is that low Zn^{2+} concentration reduce the number of spins occupying the A sublattice, causing the net magnetization to increase. As the Zn^{2+} content increases the exchange interactions are weakened and the B spins are no longer held rigidly

Table 1 Rietveld refinement results for the sample $Mg_{0.4}Zn_{0.6}NiFeO_4$

Ion	Wyck	Occ.	x	y	z
Zn^2	8a	0.570	0.00	0.00	0.00
s Fe^{3+}	8a	0.430	0.00	0.00	0.000
Mg^{2+}	16d	0.200	0.625	0.625	0.625
Zn^{2+}	16d	0.015	0.625	0.625	0.625
Ni^{3+}	16d	0.500	0.625	0.625	0.625
Fe^{3+}	16d	0.285	0.625	0.625	0.625
O^{2-}	32e	1.000	0.385	0.385	0.385

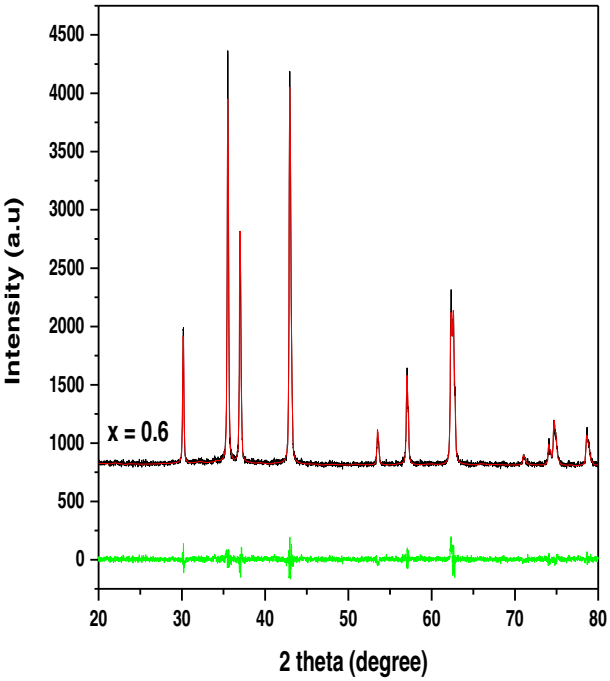

Fig. 2 Rietveld plot of the sample $Zn_{0.6}Mg_{0.4}NiFeO_4$. The points represent the measured data, the continuous line is the theoretical data and the continuous line below them is their difference

parallel to the few remaining A spins. The decrease in B sublattice moment, can be interpreted as spin departure from collinearity caused by spin canting. The canting effect was initially studied by Yafet and Kittel to interpret the spin departure by modifying the Neel's model [7]. In their interpretation they assumed that the tetrahedral and octahedral sublattices of ferrites may be subdivided into sublattices in such a way that the vector resultant of the magnetic moments of the sublattices are aligned in such directions that will influence the effective magnetism [8]. Krishna and et. al. attributed the dependence of saturation magnetization on the Zn contents to the spin-disorder and spin-canting [9]. Gismelseed [10] and Sattar [11] also described this effect for samples of Ni-Cr ferrite and Cu-Zn ferrite respectively.

Table 2 Lattice parameter constant and cation distribution of $Mg_{1-x}Zn_xNiFeO_4$

Zn content (x)	Lattice parameter (a) (Å)	Cation Distribution
0.0	8.339696	$(Mg_{0.31}Fe_{0.69})[Mg_{0.69}NiFe_{0.31}]$
0.2	8.369689	$(Mg_{0.19}Zn_{0.2}Fe_{0.61})[Mg_{0.61}NiFe_{0.39}]$
0.4	8.373944	$(Mg_{0.07}Zn_{0.4}Fe_{0.53})[Mg_{0.53}NiFe_{0.47}]$
0.6	8.375323	$(Zn_{0.57}Fe_{0.43})[Mg_{0.40}Zn_{0.03}NiFe_{0.57}]$
0.8	8.383841	$(Zn_{0.61}Fe_{0.39})[Mg_{0.20}Zn_{0.19}(Ni_{0.1})Ni_{0.9}Fe0_{.61}]$
1.0	8.385540	$(Zn_{0.64}Fe_{0.36})[Zn_{0.36}(Ni_{0.3})Ni_{0.7}Fe_{0.64}]$

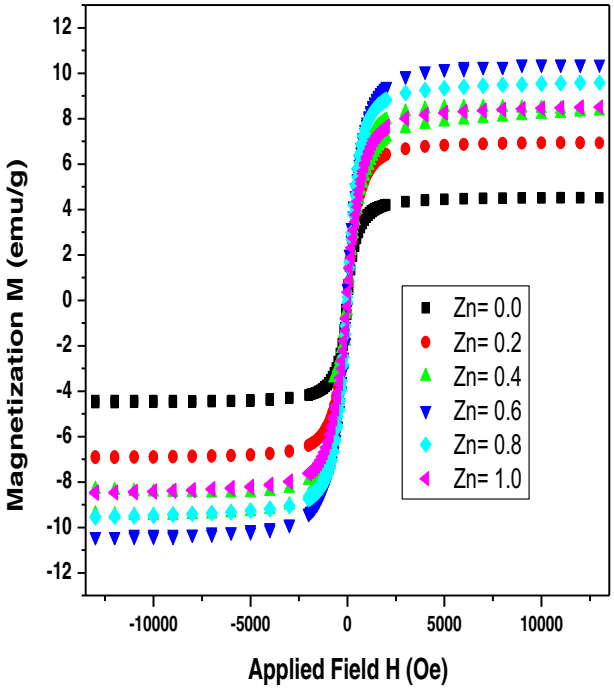

Fig. 3 Hysteresis Loops of $Zn_xMg_{1-x}NiFeO_4 (0.0 \leq \times \leq 1.0)$

The Mossbauer spectra of the $Zn_xMg_{1-x}NiFeO_4$ series, (x= 0.0 to 1.0 step 0.2) measured at 78 K are illustrated in Fig. 5, showing resolved magnetic sextets. The data were fitted by two magnetic components assigned to the two crystallographic tetrahedral (A) site and octahedral [B] site. The obtained hyperfine interaction parameters are collected in Table 3. From the Table the outer magnetic component of larger isomer shift and larger magnetic field is assigned to the octahedral site and the inner magnetic component to the tetrahedral site. These can be attributed to the cation-anion inter-nuclear separations, which are normally larger for the B-site compared to that of A-site. The linewidth broadening of the tetrahedral site for $x \geq 0.6$, is expected due to the distribution of the hyperfine magnetic field at the tetrahedral site due to the cations configuration on the octahedral crystallographic site [3].

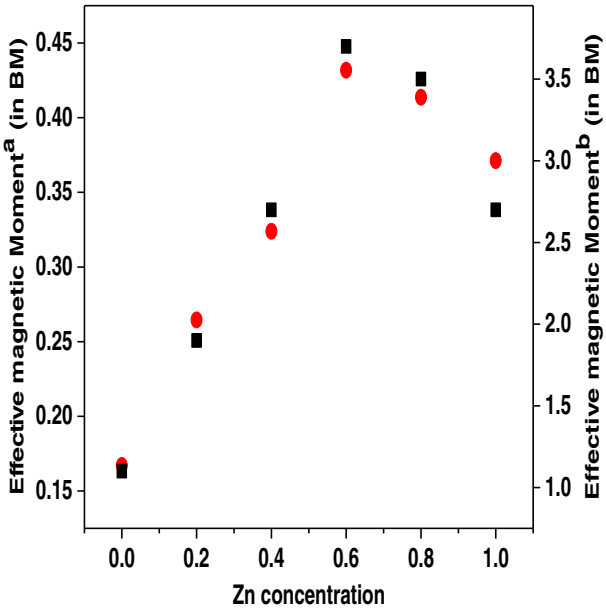

Fig. 4 Effective magnetic moments of $Zn_xMg_{1-x}NiFeO_4(0.0 \leq \times \leq= 1.0)$ versus Zn contents **a** left from VSM data **b** right; from M?ssbauer cations distribution

The magnetization of the ferrite system depends on the cations distribution and their immigration between the two crystallographic sites. Therefore, the effective magnetic moment can be calculated as a net magnetic moment per formula unit of the two crystallographic sites, using the derived cations distribution and their nonzero magnetic moment. The ionic magnetic moment of Fe^{3+}, and Ni^{3+} are $5\mu_B$ and $3\mu_B$ respectively while for Mg^{2+} and Zn^{2+} are both zero. To derive the cations distribution among the two crystallographic sites, the ratios of the areas A_A and A_B, under the resonance curve of the Mössbauer subspectra and, the recoil free fractions of Fe at the octahedral (f_B) and tetrahedral (f_A) sites (which are assumed to be equal at low temperature) were used to estimate the Fe site occupancy for each site (*i.e.* $n_A/n_B = A_A\ f_B/A_B\ \ f_A$) [12]. The Mössbauer spectra recorded at 78 K shown in Fig. 5 were used to determine the cation distribution of the series because they have better resolution compared to that measured at 295 K. As Zn^{2+} preferentially occupying the tetrahedral sites at the expense of both Mg^{2+} and Fe^{3+}, we have managed to establish the cation distribution of each sample as shown in Table 2.

From the cation distribution given in Table 2 and the values of ionic magnetic moments of Fe^{3+}, and Ni^{3+} , the effective magnetization for each content of Zn has been calculated on the basis of Neel's model, as the net magnetic moment per formula unit and the result (*right*), is plotted together with results obtained from the VSM data (*left*) in Fig. 4. As shown in the figure the effective magnetic moment has the same trend as the one obtained from the VSM measurements i.e. it starts increasing gradually to a maximum value at Zn = 0.6 following the Neel's model and then decreases with higher value of Zn content deviating

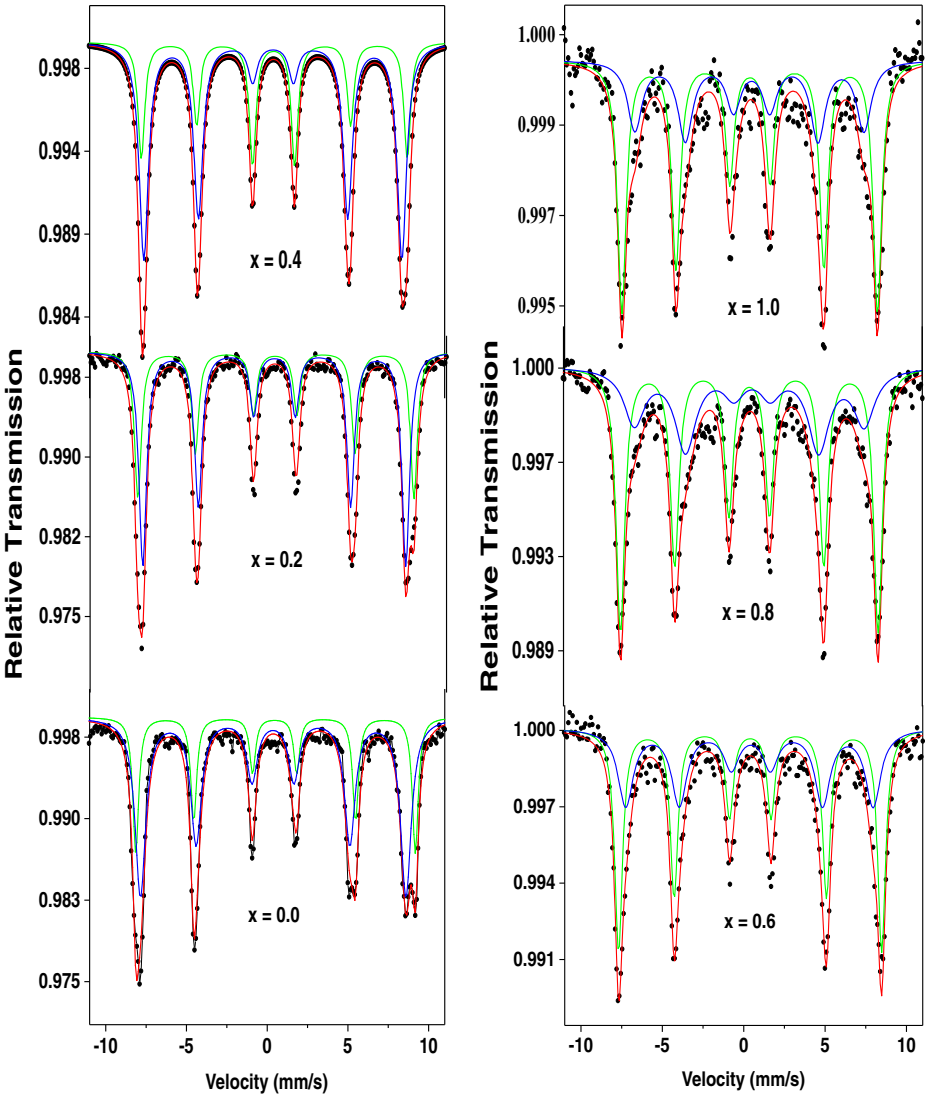

Fig. 5 Liquid Nitrogen Mössbauer spectra of $Zn_xMg_{1-x}NiFeO_4$ $(0.0 \leq \times \leq= 1.0)$

from the Neel's model. In our previous work on mixed ferrites-chromate [10], to achieve good agreement between the observed and calculated effective magnetic moment we assumed some of the Cr^{3+} moments (situated at the B-site) are aligned parallel rather than anti-parallel to the A-sites moments. Applying the same assumption for the present study, for zinc contents of more than 0.6 a fraction of Ni^{3+} ionic spins (see Table 2) will align anti-parallel to the rest of the Ni^{3+} on the B-site.

Table 3 Mössbauer hyperfine parameters at 78 K of $Mg_{1-x}Zn_xNiFeO_4$, the isomer shift δ (±0.02), quadrupole shift 2ε (±0.02), and linewidth Γ (±0.02) are in mm/s

	Tetrahedral sites (A)					Octahedral sites [B]				
X	δ	2ε	Γ	B_{hf}	A (%)	δ	2ε	Γ	B_{hf}	A(%)
0.0	0.37	0.01	0.30	51.0	69	0.49	0.03	0.22	53.7	31
0.2	0.38	−0.01	0.28	50.4	61	0.45	0.02	0.25	52.8	39
0.4	0.37	−0.02	0.30	49.0	53	0.39	0.01	0.24	51.0	47
0.6	0.40	−0.04	0.56	47.2	44	0.40	−0.01	0.29	50.1	56
0.8	0.48	−0.08	0.77	43.7	39	0.39	0.01	0.32	49.0	61
1.0	0.44	−0.06	0.77	43.7	36	0.40	−0.01	0.32	48.8	64

Magnetic field in Tesla

4 Conclusion

A series of Zinc substituted Mg-Ni ferrite were prepared by conventional double sintering ceramic method and, structurally examined by X-ray diffraction techniques confirming the formation of single cubic spinel ferrite. The value of the saturation magnetization and hence the calculated effective magnetic moment increase smoothly reaching the maximum value at Zn content of 0.6 and then decrease as Zn-content increases. The saturation magnetization results were compared with the calculated effective magnetic moment using the cations distribution driven from the resonance area of the Mössbauer subspectra of the tetrahedral and octahedral crystallographic sites. The findings of the two methods confirmed that the dependence of the magnetic properties of the series could only be explained on the basis of non-collinear spins.

Acknowledgments One of the authors (Abbasher M Gismelseed) is very grateful to the Dean's office of the college of science, Sultan Qaboos University for providing partial financial support to attend the IBAME meetings and participating the conference activities.

References

1. Aravind, G., Raghasudha, M., Ravinder, D., Manivel Raja, M., Meena, S.S., Bhatt, P., Hashim, M.: Study of structural and magnetic properties of Li-Ni nanoferrites synthesized by citrate-gel auto combustion method. Ceramics Inter. **42**, 2941–2950 (2016)
2. Velinov, N., Manova, E., Tsoncheva, T., Estournes, C., Paneva, D., Tenchev, K., Petkova, V., Koleva, K., Kunev, B., Mitov, I.: Spark plasma sintering synthesis of $Ni_{1-x}Zn_xFe_2O_4$ ferrites: Mössbauer and catalytic study. Soild State Sci. **14**, 1092–1099 (2012)
3. Gismelseed, A.M., Mohammed, K.A., Elzain, M.E., Widatallah, H.M., Al-Rawas, A.D., Yousif, A.A.: The structural and magnetic behaviour of the $MgFe_{2-x}Cr_xO_4$ spinel ferrite. Hyper. Interact. **208**, 33 (2012)
4. Lutterotti, L., Matthies, S., Wenk, H.R.: MAUD: a User friendly Java program for material analysis using diffraction. Int. Union Crystallogr. Newslett. **21**, 14 (1999)
5. Lagarec, K., Rancourt, D.G.: Rancourt, Extended Voigt-based analytic line shape method for determining N-dimensional correlated hyperfine parameter distributions in Mössbauer spectroscopy. Nucl. Instrum. Methods **129**, 266 (1998)
6. Mazen, S.A., Abu-Elsaad, N.I.: Structural and some magnetic properties of manganese-substituted lithium ferrites. J. Magn. Magn. Mater. **324**, 3366–3373 (2012)

7. Neel, L.: Magnetic Properties of Ferrites: Ferrimagnetism and Antiferromagnetism. Ann. Phys. **3**, 137 (1948)
8. Yafet, Y., Kittel, C.: Antiferromagnetic arrangements in ferrites. Phys. Rev. **87**, 290 (1952)
9. Krishna, K.R., Vijay Kumar, K., Ravindernathguta, C., Ravinder, D.: Magnetic Properties of Ni-Zn Ferrites by Citrate Gel Method. Advances in Materials Physics and Chemistry **2**, 149 (2012)
10. Gismelseed, A.M., Yousif, A.A.: Mössbauer study of chromium-substituted nickel ferrites. Phys. B **370**, 215–222 (2005)
11. Sattar, A.A., Wafik, A.H., El-Shokrofy, K.M., El-Tabby, M.M.: Magnetic Properties of Cu-Zn Ferrites Doped with rare Earth Oxides. Phys. Stat. Sol. **171**, 563 (1999)
12. Gismelseed, A.M., Widatallah, H.M., Al-Rawas, A.D., Al-Omari, I., Elzain, M.E., Yousif, A.A.: Structural characterization and magnetic properties of $NiMg_{3x/2}Cr_{0.9}Fe_{1.1-x}O_4$. Hyper. Interact. **184**, 105–110 (2008)